Biophysical Chemistry 148 (2010) 131–137

Contents lists available at ScienceDirect

Biophysical Chemistry

journal homepage: http://www.elsevier.com/locate/biophyschem

Rubredoxin mutant A51C unfolding dynamics: A Förster Resonance Energy Transfer study

Andrea Santos [a,*], Américo G. Duarte [b], Alexander Fedorov [c], José M.G. Martinho [c], Isabel Moura [b]

[a] Biomembranes Unit, Instituto de Medicina Molecular, Faculdade de Medicina, Universidade de Lisboa, Av. Professor Egas Moniz, 1649-028 Lisboa, Portugal
[b] REQUIMTE-CQFB, Departamento de Química, Faculdade de Ciências e Tecnologia, Universidade Nova de Lisboa, 2829-516 Caparica, Portugal
[c] IN-CQFM, Instituto Superior Técnico, Universidade Técnica de Lisboa, Av. Rovisco Pais, 1049-001 Lisboa, Portugal

ARTICLE INFO

Article history:
Received 25 January 2010
Received in revised form 3 March 2010
Accepted 5 March 2010
Available online 16 March 2010

Keywords:
Rubredoxin
Tryptophan
Fluorescence
FRET
Unfolding
Temperature

ABSTRACT

The unfolding dynamics of the rubredoxin mutant A51C (RdA51C) from *Desulfovibrio vulgaris* (DvRd) was studied on the temperature range from 25 °C to 90 °C and by incubation at 90 °C. By Förster Resonance Energy Transfer (FRET) the donor (D; Trp37) to acceptor (A; 1,5-IAEDANS) distance distribution was probed at several temperatures between 25 °C and 90 °C, and incubation times at 90 °C. From 25 °C to 50 °C the half-width distributions values (*hw*) are small and the presence of a discrete D–A distance was considered. At temperatures higher than 60 °C broader *hw* values were observed reflecting the existence of a distance distribution. The protein denaturation was only achieved by heating the solution for 2 h at 90 °C, as probed by the increase of the D–A mean distance. From Trp fluorescence it was shown that its vicinity was maintained until ~70 °C, being the protein hydrodynamic radius invariant until 50 °C. However, at ~70 °C a change in the partial unfolding kinetics indicates the disruption of specific H-bonds occurring in the hydrophobic core. The red shift of 13 nm, observed on the Trp37 emission, confirms the exposition of Trp to solvent after protein incubation at 90 °C for 2.5 h.

1. Introduction

Rubredoxins are a class of iron-containing proteins whose physical and chemical properties are well known [1–4]. However, the biological role of this class of proteins is still unclear, although there is evidence for their participation in electron transfer processes [5,6]. Rubredoxin structural high stability and simplicity make them suitable for studies of protein stability in extreme environmental conditions. Rubredoxins from the hyperthermophile *Pyrococcus furiosus* (PfRd), and its mesophilic analog *Clostridium pasteurianum* (CpRd) are the most studied ones, and few studies report on rubredoxin from *Desulfovibrio vulgaris* (DvRd). PfRd and CpRd particular structural features were assessed by Nuclear Magnetic Resonance (NMR) [7–10], hydrogen exchange [11,12], UV–Vis absorbance and far-UV circular dichroism [13], computational methods [14–18], Nuclear Resonance Vibrational Spectroscopy (NRVS) and Raman spectroscopy [19], and neutron crystallography [20]. The PfRd and CpRd protein unfolding mechanisms by temperature increase and/or at extreme pH or ionic strength were also studied [21–25]. The PfRd protein has a high kinetic stability compared to other mesophilic rubredoxins like CpRd. The slow unfolding rates observed for PfRd were explained by both electrostatic and hydrophobic effects. Several key surface ion pairs clamp the protein, influencing the nature and number of vibrational modes thermally accessible upon unfolding [7,21,22]. Besides this, main chain and side chain interactions between β-sheet strands and core residues can also contribute for the PfRd unusual thermal stabilization [13]. The protein hydrogen bond networking evolving the β-sheet strands and the metal binding site, as the short-range interactions between the hydrophobic core residues lateral chains, contribute significantly to the overall protein stability [8,9,14]. Solvation effects are also relevant for the stabilization of the hydrophobic core [17]. Conformational rigidity once thought to be important in hyperthermophile rubredoxins stability was recently questioned [26]. In fact, it was shown that enhanced internal protein motions may increase the stability by increasing the entropy of the native state and the melting temperature [24], while water solvation can be important in the protein internal flexibility and structural robustness [27]. However, besides several studies on PfRd stability is not possible to ascribe its unusual high stability to a single feature but rather to a wide range of factors working simultaneously [13,28–30].

Here, we studied the unfolding dynamics of the wild-type and mutant A51C rubredoxin from mesophile *Desulfovibrio vulgaris*

Abbreviations: DvRd, *Desulfovibrio vulgaris* rubredoxin; FRET, Förster Resonance Energy Transfer; D, Donor; A, Acceptor; Trp, Tryptophan; 1,5-IAEDANS, N-(iodoacetylaminoethyl)-5-naphthylamine-1-sulfonic acid; PfRd, *Pyrococcus furiosus* rubredoxin; CpRd, *Clostridium pasteurianum* rubredoxin; NMR, Nuclear magnetic resonance; NRVS, Nuclear resonance vibrational spectroscopy; Cys, Cysteine; OD, Optical density; Ala, Alanine; IPTG, Isopropyl β-D-1-thiogalactopyranoside; TCA, Trichloroacetic acid; DTT, Dithiothreitol; Asp, Aspartic acid.

* Corresponding author. Tel.: +351 21 7985136; fax: +351 21 7999477.
E-mail address: andreasantos@fm.ul.pt (A. Santos).

0301-4622/$ – see front matter © 2010 Elsevier B.V. All rights reserved.
doi:10.1016/j.bpc.2010.03.007

(DvRd), by temperature increase and by incubation at 90 °C. A combined approach including Förster Resonance Energy Transfer (FRET) experiments and tryptophan (Trp) fluorescence was used in order to obtain protein conformational dynamics data.

The DvRd is a small protein with 52 residues containing an iron–sulfur center, consisting of an iron atom coordinated by the sulfur atoms of four cysteine residues (Cys). Its structure was determined at 1.0 Å resolution (PDB entry: 8RXN, see Fig. 1) [31].

The monomeric structure consists of a three-stranded antiparallel β-sheet with a hydrophobic core containing six aromatic residues. The single tryptophan residue, Trp37, was used as energy donor in FRET experiments and as intrinsic fluorescent probe for the local environment [32–34]. As acceptor was used the N-(iodoacetylaminoethyl)-5-naphthylamine-1-sulfonic acid (1,5-IAEDANS). The donor–acceptor pair distance distribution was probed by FRET in the temperature interval between 25 °C and 90 °C, and at several incubation times between 0 and 2 h at 90 °C. These results were complemented with UV–Vis absorption, steady-state, and time-resolved fluorescence and anisotropy measurements of the single Trp37 residue.

2. Materials and methods

2.1. Protein mutagenesis and expression

The DvRd gene was previously cloned into pT7-7 vector. The single rubredoxin mutant RdA51C was obtained by site direct mutagenesis, using QuikChange® Site-Directed Mutagenesis Kit (from Stratagene). The cysteine residue was introduced on the protein surface by mutation of the alanine residue, Ala51. The Ala51 residue does not establish hydrogen bonds whose disruption could influence the protein stability and its solvent accessibility is higher than 30%. Plasmids containing the coding sequence for the DvRd and RdA51C proteins were transformed in BL21 (DE3) competent cells. The cells were grown in LB medium containing ampicillin, at 37 °C and 230 rpm. The cultures were induced by addition of isopropyl β-D-1-thiogalactopyranoside (IPTG) and let to grow over-night. The cells were harvested by centrifugation (8000×*g*; 10′, 4 °C) and ressuspended in Tris-HCl pH 7.6. Cell lyses was performed in a homogenizer (15,000 psi) and the resultant crude extract centrifuged (8000×*g*, 15′, 4 °C) to remove cell debris. The resultant supernatant was ultracentrifuged (138,000×*g*, 60′, 4 °C) and the soluble extract was loaded on a Q-Sepharose Fast Flow column (Ø 2.6×L 30 cm). Fractions containing the protein molecules were collected, concentrated by ultrafiltration, and injected in a Superdex75 column (Ø 2.6×L 70 cm). Protein purity was determined by the optical density (OD) ratio $\frac{OD_{277}}{OD_{490}}$, and its concentration calculated using the molar absorption coefficient of the oxidized form, $\varepsilon_{490\,nm} = 6{,}900\ M^{-1}\ cm^{-1}$. The protein molecular weight and theoretical isoelectric point are 5.57 KDa and 4.07, respectively.

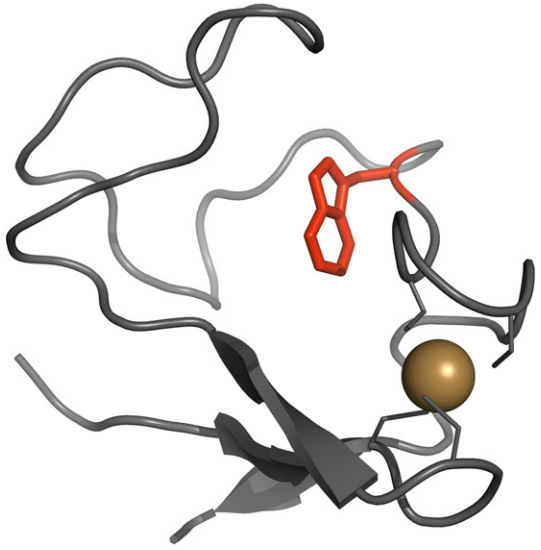

Fig. 1. DvRd folding: Trp37 (red) and metal center (yellow).

2.2. Rubredoxin labeling

The zinc substituted RdA51C protein solution (ZnRdA51C) was prepared from a rubredoxin iron solution using a protocol adapted from Moura et al. [35]. To a solution of *wt*DvRd 2 mM was added trichloroacetic acid (TCA) 5% (w/w) and dithiothreitol (DTT) 0.5 M. The mixture was heated to 45 °C during 1 h, centrifuged and the precipitate dissolved in a Tris-base 0.5 M plus DTT 60 mM solution. In a vacuum chamber the apo-DvRd protein was purified by gel filtration and a solution of $ZnCl_2$ was stoichiometrically added. Rubredoxin alkylation process was done following the protocol described by Crankshaw and Grant [36]. The N-(iodoacetylaminoethyl)-5-naphthylamine-1-sulfonic acid (1,5-IAEDANS) dye was labeled to the mutated cysteine residue (Cys51) located in the protein surface. This dye was chosen as acceptor due to its large Stokes shift and good spectral overlap of its absorption band with the emission of Trp37 [37]. Besides this, its fluorescence is less dependent on environment when compared to other conjugates and is characterized by a relatively long mean fluorescence lifetime ($\overline{\tau}\sim 12$ ns). The RdDv:IAEDANS ratio, found to be ~1, was calculated by UV absorption using the molar absorption coefficients, $\varepsilon_{280\,nm} = 10{,}220\ M^{-1}\ cm^{-1}$ for the protein, and $\varepsilon_{278\,nm} = 1{,}060\ M^{-1}\ cm^{-1}$ and $\varepsilon_{337\,nm} = 6{,}100\ M^{-1}\ cm^{-1}$ for IAEDANS [38].

2.3. Fluorescence measurements

The fluorescence spectra were recorded in a spectrofluorimeter Fluorolog 3 (from Spex). The spectra recorded by excitation at $\lambda_{exc} = 280$ nm were corrected for the response of the fluorescence detecting system using a correction curve included in the software package equipment. The temperature was controlled within ±0.5 °C with a K-16212 thermometer (from Bioblock) and the solutions were stirred during the measurements.

2.4. Time-Correlated Single-Photon Counting

The fluorescence decay curves were obtained by the Time-Correlated Single-Photon Counting (TCSPC) technique using picosecond laser excitation. The 280 nm excitation pulse (5–6 ps) was achieved by doubling the laser output light of a Coherent 701-2 dye (Rhodamine 6G) laser synchronously pumped by a mode-locked Coherent Innova 400-1 argon ion laser. The excitation light beam was expanded before entering the sample solution and neutral density filters were used in order to minimize the photodegradation of rubredoxin. The fluorescence was selected by a Jovin-Yvon HR320 monochromator with a grating of 100 lines mm^{-1} (20 nm bandwidth) and detected by a Hamamatsu 2809U-01 microchannel plate photomultiplier. The fluorescence decay curves were acquired using vertical polarized light for excitation and selecting the fluorescence at the magic angle (54.7°). The decay curves were fitted with a sum of exponentials plus a constant,

$$I(t) = \sum_i a_i \exp\left(-\frac{t}{\tau_i}\right) + a_0 \qquad (1)$$

where a_i, τ_i are the amplitude and lifetime, respectively, of the i^{th} decay component and a_0 a scattering component that accounts for the scattered light and very fast processes unresolved by our TCSPC equipment [39]. The anisotropy decay curves $r(t)$ were constructed from the $I_{VV}(t)$ and $I_{VH}(t)$ fluorescence decays obtained with vertical

polarized excitation light and selecting the vertical (I_{VV}) or horizontal (I_{VH}) components of the fluorescence,

$$r(t) = \frac{I_{VV}(t) - GI_{VH}(t)}{I_{VV}(t) + 2GI_{VH}(t)} \quad (2)$$

where $G = \frac{I_{HV}}{I_{HH}}$ is an experimental correction factor that considers the artifacts introduced by the detecting system on the polarized fluorescence light components. For our experimental set-up $G = 1$ because the fluorescence after being selected with an appropriate polarizer was depolarized before the entrance slit of the monochromator. The fluorescence anisotropy decay was fitted with a mono-exponential,

$$r(t) = r_0 \exp\left(-\frac{t}{\theta}\right) \quad (3)$$

where r_0 is the anisotropy at time zero and θ is the rotational correlation time. The fittings were performed by a nonlinear least-squares method based on the Marquard algorithm [40] and the quality of the fit was judged by the reduced χ^2 (~1), weighted residuals (random ~0) and autocorrelation of the residuals.

2.5. FRET experiments

The distance between the donor (D; Trp37) and acceptor (A; IAEDANS) was determined using the fluorescence decay curves obtained from unlabeled and labeled ZnRdA51C protein solutions (10 μM; pH 8). The fluorescence decay curves of the donor-alone were fitted with Eq. (1). The distance-dependent donor decay of a donor–acceptor pair separated by a single distance r is given by,

$$I_{DA}(r,t) = \sum_i a_i \exp\left[-\frac{t}{\tau_i} - \frac{t}{\tau_i}\left(\frac{R_0}{r}\right)^6\right] \quad (4)$$

where R_0 is the critical Förster radius [41]. The second term of the exponent considers the rate of energy transfer for each of the Trp conformers, $k_{DA} = \frac{1}{\tau_D}\left(\frac{R_0}{r}\right)^6$. If a distribution of separations exists between the D–A FRET pair then,

$$I_{DA}(t) = \int_0^\infty P(r) I_{DA}(r,t) dr \quad (5)$$

where $P(r)$ is the probability distribution function for the separation assumed to be a Gaussian function,

$$P(r) = \frac{1}{\sigma\sqrt{2\pi}} \exp\left[-\frac{1}{2}\left(\frac{r-\overline{r}}{\sigma}\right)^2\right] \quad (6)$$

where $\overline{r}$ is the mean distance and σ is the standard deviation of the distribution. The half-width (hw) of the distribution is given by $hw = 2.354\sigma$. The program CFS_LS/GAUDIS was used to determine the distance distribution from Eq. (5) and assuming incomplete labeling of the acceptor site [42].

The critical Förster radius, R_0 was calculated from the donor and acceptor spectral properties,

$$R_0 = 0.211\left(\frac{\kappa^2 \phi_D J(\lambda)}{n^4}\right)^{1/6} \quad (7)$$

where κ^2 is a factor describing the relative orientation in space of the transition dipoles for the donor and acceptor ($\kappa^2 = 2/3$), ϕ_D is the quantum yield of the donor in the absence of acceptor ($\phi_D \sim 0.12$), n is the refractive index of the medium and J the overlap integral,

$$J(\lambda) = \int F_D(\lambda)\varepsilon_A(\lambda)\lambda^4 d\lambda \quad (8)$$

where $F_D(\lambda)$ is the corrected fluorescence intensity of the donor at the wavelength λ with area normalized to unity, $\varepsilon_A(\lambda)$ is the extinction coefficient of the acceptor. The R_0 value was considered equal for all Trp conformers and for each donor–acceptor pair in the analysis, irrespective of the lifetime.

3. Results and discussion

3.1. UV–VIS spectra

Fig. 2 shows the UV–Vis absorption spectra of RdA51C solutions (10 μM; pH 8) at 25 °C and 90 °C, and incubated at 90 °C during 2.5 h.

The UV–Vis spectrum of the mutant is composed of four main bands with maxima at 279, 378, 493 and 570 nm, characteristic of rubredoxins [1]. The first band at 279 nm results from the four aromatic residues Tyr4, Tyr11, Tyr13 and Trp37. The last three bands are sulfur-to-iron charge transfer bands involving at least one cysteine ligand. With temperature increase, the charge transfer bands decrease in intensity reflecting the loss of iron from the protein (see Fig. 2). The iron release occurs continuously being more pronounced at higher temperatures. The iron release is complete after 2.5 h of incubation.

3.2. Fluorescence spectra

The fluorescence spectra of ZnRdA51C solutions were obtained from 25 °C to 90 °C and during time at 90 °C, by excitation at $\lambda_{exc} = 280$ nm (Fig. 3). The paramagnetic iron ion that quenches efficiently the tryptophan fluorescence was substituted by zinc without considerable change of the protein structure [9,10].

The ZnRdA51C protein fluorescence shows a single band with maximum at 315 nm, in the 25 °C to 90 °C temperature range, attributed to the Trp37 fluorescence. The fluorescence maximum at 315 nm indicates that the single tryptophan residue is located in a hydrophobic environment (<20% water) [43]. No solvatochromic shift was observed on the fluorescence maximum, despite a slight broadening and intensity decrease at high temperatures. This means that Trp37 local environment does not change significantly with temperature. The interactions involving the first 15 residues and inside the hydrophobic core seems to play an important role in the high structural stability of rubredoxins and can justify the above observations [9,13,14]. Indeed, Bougault et al. observed by NMR that two strong H-bonds between Cys6 → Tyr11 and Tyr13 → Tyr4 remain intact until 70 °C in both CpRd and PfRd proteins [8]. As these residues are conserved in DvRd structure it's also expected that they will contribute for the protein high stability.

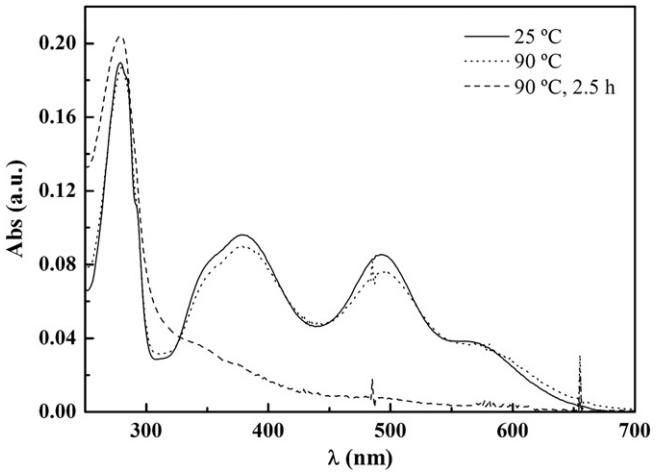

Fig. 2. UV–Vis spectra of RdA51C solutions (10 μM; pH ~8) at 25 °C (—), 90 °C (–) and 90 °C for 2.5 h (….).

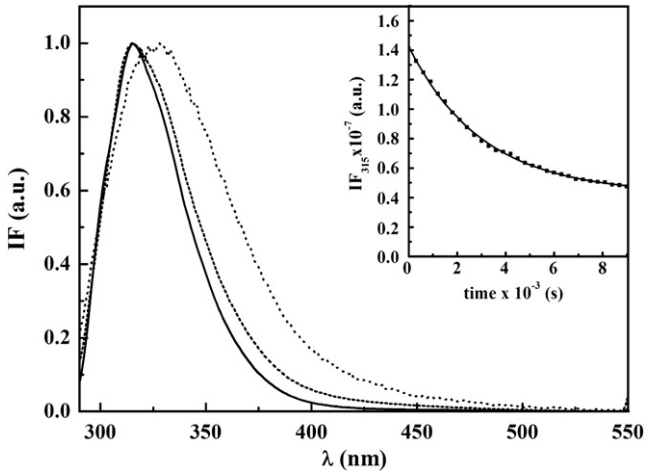

Fig. 3. Normalized emission spectra of ZnRdA51C solutions (10 μM; pH ~ 8) obtained at 25 °C (—), 90 °C (--) and 90 °C for 2.5 h (….), $\lambda_{exc} = 280$ nm. Insert: fluorescence intensity at 315 nm vs. time, at 90 °C, and fit (—).

After 2.5 h of incubation at 90 °C a red shift of ~13 nm was observed on the Trp37 emission (see Fig. 3). This solvatochromic shift on the emission spectra clearly indicates a partial exposition of Trp37 residue to the solvent. Protein unfolding starts by the separation of two loops and exposure of the hydrophobic core, followed by unzipping of the β-sheet [24]. The Trp37 vicinity becomes more hydrophilic but this residue is not fully exposed to solvent upon protein unfolding. From the time-evolution of the fluorescence intensity maximum and by fitting the equation $IF_{obs} = IF_0 \exp(-k_{unf}t) + a$, an apparent first-order unfolding rate constant of $k_{unf} = 3.27 \pm 0.06 \times 10^{-4}\ s^{-1}$ was obtained (see insert in Fig. 3). This value is intermediate between those obtained for CpRd ($k_{unf} = 3.9 \times 10^{-3}\ s^{-1}$) and PfRd ($k_{unf} = 1.9 \times 10^{-6}\ s^{-1}$) [21].

3.3. Fluorescence decays

The fluorescence decays of ZnRdA51C solutions (10 μM; pH 8) were obtained from 25 °C to 90 °C, by $\lambda_{exc} = 280$ nm and recording the emission at $\lambda_{em} = 330$ nm. These decays were analyzed with a sum of two or three exponentials plus a scattering component (Eq. (1)). The obtained normalized pre-exponential values (a_i), lifetimes (τ_i), mean lifetimes ($\tau_m = \frac{\sum a_i \tau_i}{\sum a_i}$) and chi-squares ($\chi^2$) are shown in Table 1.

The lifetimes obtained at 25 °C are identical to those obtained for the wild-type protein which indicates that the mutation does not influence Trp37 vicinity (values not shown). Between 25 °C and 60 °C two lifetimes were recovered and at higher temperatures a three exponential fit is required to obtained random distributed residuals and $\chi^2 \sim 1$. The observed fluorescence heterogeneity was attributed to the existence of tryptophan rotational isomers, and/or to ground-state heterogeneity due to multiple protein conformations and distinct fluorescence quenching mechanisms that the peptide bond and residues in the vicinity exert on the tryptophan fluorescence [44,45]. A probable quenching process of the Trp37 fluorescence is due to the formation of an H-bond between the Trp37 indole NH and a carboxylate oxygen of the side chain of the aspartic acid residue Asp19, that apparently disappears at temperatures higher than 75 °C [24,25]. By formation of this H-bond the Asp19 residue becomes close to Trp37 residue and quenches its emission by an electron transfer mechanism. At 70 °C a third lifetime of 0.14 ns was observed. This component results from a strong quenching mechanism activated at higher temperatures. The disulfide bridge with a quenching rate of $k_q \sim 10^{10}\ M^{-1}\ s^{-1}$ is a strong candidate [45]. Indeed, by metal release the cysteine residues involved in the metal center can react to form disulphide bridges given rise to the appearance of this short lifetime component at 70 °C.

Fig. 4 shows the Arrhenius plot, $k = A \exp\left(-\frac{E_a}{RT}\right)$ of the reciprocal of the average lifetime.

A break was observed at 70 °C, suggesting a change in the dynamic quenching processes and consequently on the protein dynamics regime, around this temperature. For temperatures below 70 °C the fit allows the calculation of the pre-exponential factor, A and activation energy, E_a of $382.9 \pm 22.5\ s^{-1}$ and 16.1 ± 0.2 kJ mol^{-1}, respectively. Above 70 °C, both values increase to $6.0 \pm 1.2 \times 10^3\ s^{-1}$ and 23.9 ± 0.6 kJ mol^{-1}, respectively. By dynamic simulations performed with the DvRd protein it was shown that the loop region comprising the residues 16–47 (where Trp37 is inserted) is the most labile especially at the rim of the hydrophobic core (residues 22 and 37) [24]. These observations in addition with the break of the H-bonds Cys6 → Tyr11, Tyr13 → Tyr4, and Trp37 → Asp19 at temperatures higher than 70 °C, should be the main reasons for the observed Arrhenius type behavior [8,24,25].

From the fluorescence decays of ZnRdA51C solutions (10 μM; pH 8) obtained by incubation at 90 °C between 0 and 2.5 h, three components of ~ 1 ns, 0.3 ns and 0.06 ns with small variations in their amplitudes were recovered at all instants. The mean lifetime slightly increased in time stabilizing ~0.48 ns after 1.5 h of incubation. The invariance of the lifetimes with time is consistent with the existence of a strong quenching mechanism active at higher temperatures. As reported before, the Trp fluorescence quenching by the cysteine residues Cys39 and Cys42, is the most probable one. In fact this mechanism is equally efficient in the folded and denatured protein because the cystine and cysteine residues quenching rates are both very high [45]. However, the Trp quenching by the Asp36 residue, through an electron transfer mechanism, should also be considered.

Table 1
Normalized pre-exponential values (a_i), lifetimes (τ_i), mean lifetimes (τ_m) and chi-squares (χ^2) of ZnRdA51C solutions (10 μM; pH 8) at 25 °C to 90 °C ($\lambda_{exc} = 280$ nm; $\lambda_{em} = 330$ nm).

T (°C)	a_1	τ_1 (ns)	a_2	τ_2 (ns)	a_3	τ_3 (ns)	τ_m (ns)	χ^2
25	0.64	1.89	0.36	1.09			1.69	1.23
30	0.55	1.75	0.45	1.07			1.53	1.16
40	0.21	1.73	0.79	1.04			1.25	1.12
50	0.34	1.35	0.66	0.71			1.03	1.12
60	0.14	1.42	0.86	0.65			0.85	1.14
70	0.07	1.51	0.72	0.56	0.21	0.14	0.73	1.01
80	0.042	1.44	0.71	0.45	0.25	0.13	0.57	1.04
90	0.102	0.87	0.67	0.32	0.23	0.073	0.46	1.00

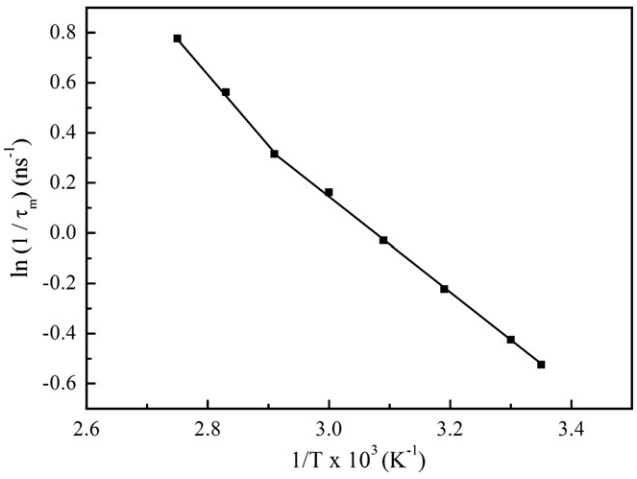

Fig. 4. Arrhenius plot for the partial unfolding of ZnRdA51C protein on the temperature range from 25 °C to 90 °C.

3.4. Anisotropy decays

The anisotropy decays of ZnRdA51C solutions (10 μM; pH ~ 8) were obtained in the temperature range between 25 °C and 90 °C. The anisotropy decay curves, $r(t)$, were constructed from the I_{VV} (t) and I_{VH} (t) fluorescence decays using Eq. (2) and were well fitted with Eq. (3). Table 2 summarizes the rotational correlation times (θ) and anisotropies at time zero (r_0) obtained at several temperatures.

The rotational correlation time was associated with the rotation of the protein as a whole in the temperature range from 25 °C to 50 °C, where its value is constant (~2.6 ns). Assuming a spherical shape of the protein, the correlation time is given by,

$$\theta = \frac{\eta V}{RT} \tag{9}$$

where, η is the solvent viscosity (9.55×10^{-4} Pa.s), V the molar volume of the protein ($m^3\ mol^{-1}$), T the absolute temperature (298.15 K) and R the ideal gas constant ($8.31\ JK^{-1}\ mol^{-1}$). Using the correlation time value at 25 °C, the protein hydrodynamic radius was estimated, $R_h = 14.3$ Å. The crystallographic value is smaller ~12.5 Å and the difference is due to the protein hydration.

The correlation times retrieved between 60 °C and 90 °C reflect the dynamics of the segmental region where the tryptophan residue is inserted. If fast motions occurs they should be to fast to be detected by our experimental set-up.The H-bond network weakening or even its break with temperature increase is the main cause for the decrease in the observed θ values.

At room temperature the anisotropy at zero time is ~0.10. The r_0 value includes contributions from both ^1L_a and ^1L_b excited states of indole at $\lambda_{exc} = 280$ nm. At this wavelength the expected r_0 value for indole in vitrified propylene glycol is 0.15 [32]. As the obtained r_0 values don't vary with temperature the difference should be due to scattering or very fast relaxation processes occurring in a very fast time scale not detectable by the experimental set-up [33].

3.5. FRET experiments

The donor-alone and donor in the presence of acceptor decays were obtained in the temperature range from 25 °C to 90 °C and at several incubation times at 90 °C, using $\lambda_{exc} = 280$ nm and $\lambda_{em} = 330$ nm. The Trp fluorescence decay curves obtained for labeled and unlabeled rubredoxin at 25 °C are shown on Fig. 5.

The rubredoxin–IAEDANS Trp decay curve is faster which indicates energy transfer between the donor and acceptor. The donor-alone fluorescence decay curve was fitted by a nonlinear least-squares method using Eq. (1). The recovered donor-alone lifetimes were further used on the CFS_LS/GAUDIS nonlinear least-squares fit of donor–acceptor fluorescence decay. The obtained distribution parameters, $\overline{r}$ and *hw*, are sumarized on Table 3 for the temperature range from 25 °C to 90 °C and on Table 4 for several incubation times at 90 °C.

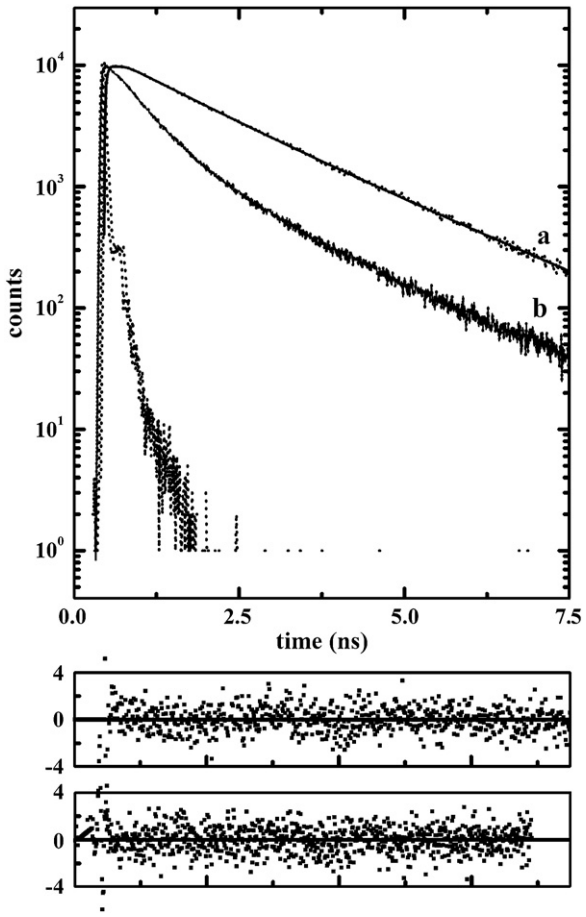

Fig. 5. Fluorescence decay curves of mutant rubredoxin solutions (10 μM; pH 8) obtained at 25 °C with $\lambda_{exc} = 280$ nm and $\lambda_{em} = 330$ nm. (....) laser profile. Curve *a* is the decay from the donor-alone sample and the fit (—) with Eq. (1). Curve *b* is the decay from the donor–acceptor sample and the fit (—) with Eq. (5). The lower panel are the residuals for the fits shown in curves *a* and *b*.

A Förster critical radius, $R_0 = 21.8$ Å, was considered in all calculations, which is reasonable since both the fluorescence–absorption overlap integral and the donor quantum yield do not vary significantly with temperature (results not shown). Besides this, the $P(r)$ estimation is more affected by orientational disorders and the probe linker arm that directly contribute to increase the distribution half-width, *hw*. An orientation factor $\kappa^2 = 2/3$ was used since the IAEDANS rotational motion is random in the protein. The probability distribution function, $P(r)$ determined from Eq. (6) is shown in Fig. 6 for 25 °C, 90 °C and after incubation at 90 °C for 2 h.

The mean donor–acceptor distance, $\overline{r}$ slightly varied between 25 °C and 50 °C and the distribution is characterized by small half-widths, *hw* (Table 3). In this temperature interval the rubredoxin fold

Table 2
Anisotropy at time zero (r_0), rotational correlation time (θ) and hydrodynamic radius (R_h) of ZnRdA51C solutions (10 μM; pH 8) at 25 °C to 90 °C ($\lambda_{exc} = 280$ nm; $\lambda_{em} = 330$ nm).

T (°C)	r_0	θ (ns)	R_h (Å)
25	0.095	2.84	14.3
30	0.120	2.62	14.0
40	0.109	2.65	14.2
50	0.109	2.43	13.9
60	0.103	1.41	
70	0.089	0.80	
80	0.092	0.86	
90	0.098	1.49	

Table 3
Donor–acceptor mean distance ($\overline{r}$), distance distribution half-width (*hw*) and chi-square (χ^2) for ZnRdA51C–IAEDANS pair at 25 °C to 90 °C ($\lambda_{exc} = 280$ nm; $\lambda_{em} = 330$ nm).

T (°C)	$\overline{r}$(Å)	*hw* (Å)	χ^2
25	18.84 ± 0.05	2.03 ± 0.36	1.19
30	19.02 ± 0.01	~0	1.11
40	19.64 ± 0.02	1.03 ± 0.16	1.17
50	20.37 ± 0.01	~0	1.26
60	21.47 ± 0.15	7.55 ± 0.29	1.00
70	24.12 ± 0.02	7.15 ± 0.10	1.07
80	25.87 ± 0.06	8.39 ± 0.60	1.16
90	23.96 ± 0.09	8.44 ± 0.13	1.16

Table 4
Donor–acceptor mean distance ($\overline{r}$), distance distribution half-width (*hw*), and chi-square (χ^2) for ZnRdA51C–IAEDANS pair at 90 °C, from 0 to 2 h (λ_{exc} = 280 nm; λ_{em} = 330 nm).

Time (h)	$\overline{r}$ (Å)	*hw* (Å)	χ^2
0.0	24.67 ± 0.05	9.22 ± 0.30	1.08
0.5	25.92 ± 0.09	28.48 ± 0.29	1.20
1.0	26.63 ± 0.01	6.61 ± 0.21	1.15
1.5	25.98 ± 0.05	8.07 ± 0.01	1.22
2.0	27.82 ± 0.07	7.55 ± 0.31	1.08

is maintained with minor structural deviations. This was previously observed by the invariance of the rubredoxin circular dichroism spectra obtained in the same temperature interval (data not shown). From the anisotropy measurements a similar conclusion was taken when a constant hydrodinamic radius of ~14 Å was obtained in the same temperature interval. The small *hw* values reveal the presence of discrete donor–acceptor distances, probably due to the low protein structure flexibility. The difference between the crystalographic separation of Cys51 and Trp37 (12–16 Å) and the mean distance at 25 °C accounts for protein hydration plus the probe linker arm. At temperatures higher than 50 °C both $\overline{r}$ and *hw* values increase (see Table 3). The acceptor molecule is attached close to the C-terminal, a high mobile structural element that should become more labile and extend to the solvent as the temperature is raised, resulting in higher $\overline{r}$ values. The broader *hw* values reflect an increase on the protein structure flexibility and can have several origins like protein conformational heterogeneity, different orientation factor values, and probe linker arm rotation. The Trp rotational motions in the same order of magnitude as its lifetimes (θ ~ 0.8–1.5 ns), also contribute to the *hw* value increase.

A very broad distribution of separations was obtained after 0.5 h incubation at 90 °C (see Table 4). This was attribute to the co-existence of native-like, partially denatured and unfolded protein molecules, in addition to the orientational disorders and probe linker arm effects. After 2 h incubation, the donor–acceptor mean distance was shifted to larger values (27.8 Å) and the *hw* value was reduced (~8 Å). The $\overline{r}$ ~ 28 Å is consistent with the expected theoretical value for a random coil configuration. The average distance between two residues in an unfolded protein separated by 13 residues along the protein chain is given by $R(\text{coil}) = 5.45 \times (51\text{–}37)^{1/2} = 20.4$ Å [46]. Taking into account the linker arm composed of nine single bonds between the α-carbon of the mutated residue Cys51 and the acceptor fluorophore, a length of 8.5 ± 1.5 Å should be added to the R(coil) value [47]. From these data it was concluded that the majority of the protein molecules unfolds after 2 h incubation at 90 °C, and adopt a random coil configuration.

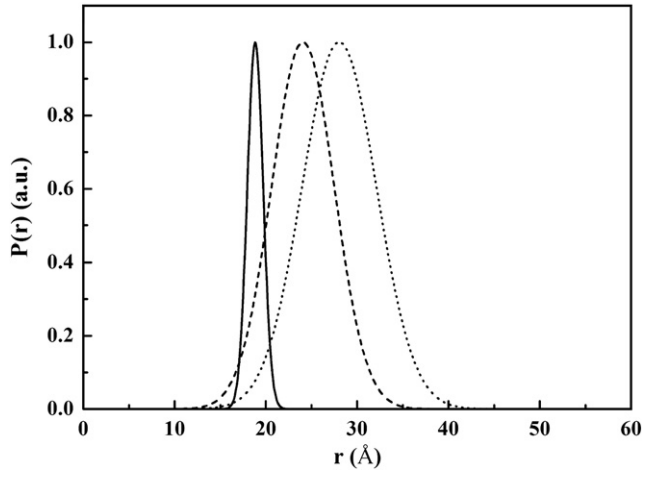

Fig. 6. Peak normalized probability of distance distributions, $P(r)$ for mutant rubredoxin solutions at 25 °C (—), 90 °C (--) and 90 °C for 2.5 h (….).

4. Conclusions

Using a FRET approach the conformational dynamics of the DvRd protein was studied at several temperature values between 25 °C and 90 °C, and at different incubation times at 90 °C. The energy transfer measurements confirm the integrity of the protein by temperature increase until 90 °C. The small variation observed on the donor–acceptor distance with temperature was attributed to the flexibility of the protein C-terminal where the acceptor is located. The unfolded protein, obtained by incubation at 90 °C for 2 h, adopts a random coil configuration as suggested by the agreement between the donor–acceptor mean distance obtained by FRET and the value calculated assuming a random-coil configuration of the protein taking into account the linker arm length. Probing the Trp37 fluorescence it was observed that the Trp remains buried in a highly hydrophobic environment at all temperatures before unfolding. Upon protein unfolding the Trp37 vicinity becomes more hydrophilic but this residue is not fully exposed to solvent. At 70 °C the appearance of a short lifetime on the Trp decay is related to protein metal release. H-bond breaking at temperatures higher than 70 °C is reflected in a kinetic regime change of the protein conformational dynamics.

Acknowledgments

We thank financial support from Fundação para a Ciência e Tecnologia (FCT) under project POCTI/QUI/64638/2006. Andrea M. Santos thanks FCT for the post-doc grant SFRH/BPD/26821/2006. Américo G. Duarte thanks FCT for the Ph.D. grant SFRH/BD/39009/2007.

Appendix A. Supplementary data

Supplementary data associated with this article can be found, in the online version, at doi:10.1016/j.bpc.2010.03.007.

References

[1] J. Meyer, J.-M. Moulis, in: A. Messerschmidt, R. Huber, K. Wieghardt, T. Poulos (Eds.), Handbook of Metalloproteins, Rubredoxin, vol. 1, John Wiley & Sons, 2001, p. 505.
[2] W. Lovenberg, M.N. Walker, Rubredoxin, Methods Enzymol. 53 (1978) 340–346.
[3] L.C. Sieker, R.E. Stenkamp, J. LeGall, Rubredoxin in crystalline state, Methods Enzymol. 243 (1994) 203–216.
[4] F.E. Jenney, M.W. Adams, Rubredoxin from *Pyrococcus furiosus*, Methods Enzymol. 334 (2001) 45–55.
[5] R. Kümmerle, H. Zhuang-Jackson, J. Gaillard, J.-M. Moulis, Site-directed mutagenesis of rubredoxin reveals the molecular basis of its electron transfer properties, Biochemistry 36 (1997) 15983–15991.
[6] E.D. Coulter, D.M. Kurtz, A role for rubredoxin in oxidative stress protection in *Desulfovibrio vulgaris*: catalytic electron transfer to rubrerythrin and two-iron superoxide reductase, Arch. Biochem. Biophys. 394 (2001) 76–86.
[7] P. Strop, S.L. Mayo, Contribution of surface salt bridges to protein stability, Biochemistry 39 (2000) 1251–1255.
[8] C.M. Bougault, M.K. Eidsness, J.H. Prestegard, Hydrogen bonds in rubredoxins from mesophilic and hyperthermophilic organisms, Biochemistry 42 (2003) 4357–4372.
[9] E.R. Zartler, F.E. Jenney, M. Terrell, M.K. Eidsness, M.W. Adams, J.H. Prestegard, Structural basis for thermostability in aporubredoxins from *Pyrococcus furiosus* and *Clostridium pasteurianum*, Biochemistry 40 (2001) 7279–7290.
[10] P. Blake, J. Park, Z. Zhou, D. Hare, M. Adams, M. Summers, Solution-state structure by NMR of zinc-substituted rubredoxin from the marine hyperthermophilic archaebacterium *Pyrococcus furiosus*, Prot. Sci. 1 (1992) 1508–1521.
[11] R. Hiller, Z.H. Zhou, W.W. Adams, S.W. Englander, Stability and dynamics in a hyperthermophilic protein with melting temperature close to 200 °C, Proc. Natl. Acad. Sci. 94 (1997) 11329–11332.
[12] G. Hernández, F.E. Jenney, M.W. Adams, D.M. LeMaster, Millisecond time scale conformational flexibility in a hyperthermophile protein at ambient temperature, Proc. Natl. Acad. Sci. 97 (7) (2000) 3166–3170.
[13] M.K. Eidsness, K.A. Richie, A.E. Burden, D.M. Kurtz, R.A. Scott, Dissecting contributions to the thermostability of *Pyrococcus furiosus* rubredoxin: β-sheet chimeras, Biochemistry 36 (1997) 10406–10413.

[14] J. Vondrášek, L. Bendová, V. Klusák, P. Hobza, Unexpectedly strong energy stabilization inside the hydrophobic core of small protein rubredoxin mediated by aromatic residues: correlated *ab initio* quantum chemical calculations, J. Am. Chem. Soc. 127 (2005) 2615–2619.
[15] M. Sundararajan, I.H. Hillier, N.A. Burton, Structure and redox properties of the protein, rubredoxin, and its ligand and metal mutants studied by electronic structure calculation, J. Phys. Chem. A 110 (2006) 785–790.
[16] D.H. Jung, N.S. Kang, M.S. Jhon, Site-directed mutation study on hyperthermostability of rubredoxin from *Pyrococcus furiosus* using molecular dynamics simulations in solution, J. Phys. Chem. A 101 (1997) 466–471.
[17] K.E. Riley, K.M. Merz, Role of solvation in the energy stabilization inside the hydrophobic core of the protein rubredoxin, J. Phys. Chem. B 110 (2006) 15650–15653.
[18] I. Tavernelli, E.E. Di Iorio, The interplay between dynamics and frustration of non-bonded interactions as revealed by molecular dynamics simulations, Chem. Phys. Lett. 345 (2001) 287–294.
[19] Y. Xiao, H. Wang, S.J. George, M.C. Smith, M. Adams, F. Jenney, W. Sturhahn, E. Alp, J. Zhao, Y. Yoda, A. Dey, E. Solomon, S. Cramer, Normal mode analysis of *Pyrococcus furiosus* rubredoxin via Nuclear Resonance Vibrational Spectroscopy (NRVS) and Resonance Raman Spectroscopy, J. Am. Chem. Soc. 127 (2005) 14596–14606.
[20] T. Chatake, A. Ostermann, K. Kurihara, F.G. Parak, N. Niimura, Hydration in proteins observed by High-Resolution Neutron Crystallography, Proteins 50 (2003) 516–523.
[21] S. Cavagnero, D.A. Debe, Z.H. Zhou, M.W. Adams, S.I. Chan, Kinetic role of electrostatic interactions in the unfolding of hyperthermophilic and mesophilic rubredoxins, Biochemistry 37 (1998) 3369–3376.
[22] S. Cavagnero, Z.H. Zhou, M.W. Adams, S.I. Chan, Unfolding mechanism of rubredoxin from *Pyrococcus furiosus*, Biochemistry 37 (1998) 3377–3385.
[23] P. Strop, S.L. Mayo, Rubredoxin variant folds without iron, J. Am. Chem. Soc. 121 (1999) 2341–2345.
[24] T. Lazaridis, I. Lee, M. Karplus, Dynamics and unfolding pathways of a hyperthermophilic and a mesophilic rubredoxin, Prot. Sci. 6 (1997) 2589–2605.
[25] F. Bonomi, D. Fessas, S. Iametti, D. Kurtz, S. Mazzini, Thermal stability of *Clostridium pasteurianum* rubredoxin: deconvoluting the contributions of the metal site and the protein, Prot. Sci. 9 (2000) 2413–2426.
[26] R. Jaenicke, Do ultrastable proteins from hyperthermophiles have high or low conformational rigidity? Proc. Natl. Acad. Sci. 97 (2000) 2962–2964.
[27] F. Sterpone, C. Bertonati, G. Briganti, S.J. Melchionna, Key role of proximal water in regulating thermostable proteins, Phys. Chem. B 113 (2009) 131–137.
[28] R.M. Daniel, M. Dines, H.H. Petach, The denaturation and degradation of stable enzymes at high temperatures, Biochem. J. 317 (1996) 1–11.
[29] R. Jaenicke, G. Böhm, The stability of proteins in extreme environments, Curr. Opin. Struct. Biol. 8 (1998) 738–748.
[30] C. Vieille, G.J. Zeikus, Hyperthermophilic enzymes: sources, uses, and molecular mechanisms for thermostability, Microbiol. Mol. Biol. Rev. 65 (2001) 1–43.
[31] Z. Dauter, L.C. Sieker, K.S. Wilson, Refinement of rubredoxin from *Desulfovibrio vulgaris* at 1.0 Å with and without restraints, Acta Crystallogr. Sect. B Strct. Commun. 48 (1992) 42–59.
[32] J.R. Lakowicz, Principles in Fluorescence Spectroscopy, Springer, New York, 2006.
[33] B. Valeur, Molecular Fluorescence, Wiley-VCH, Germany, 2002.
[34] P. Selvin, The renaissance of fluorescence resonance energy transfer, Nat. Struct. Biol. 7 (2000) 730–734.
[35] I. Moura, M. Teixeira, J. LeGall, J. Moura, Spectroscopic studies of cobalt and nickel substituted rubredoxin and desulforedoxin, J. Inorg. Biochem. 44 (1991) 127–139.
[36] M.W. Crankshaw, G.A. Grant, Current Protocols in Protein Science, Modification of Cysteine, John Wiley & Sons, New York, 1996, p. 15.1.1.
[37] Thiol-Reactive Probes. Molecular Probes: The Handbook [Online]; InvitrogenTM http://www.invitrogen.com/site/us/en/home/References/Molecular-Probes-The-Handbook.
[38] E.N. Hudson, G. Weber, Synthesis and characterization of two fluorescent sulfhydryl reagents, Biochemistry 12 (1973) 4154–4161.
[39] J.M.G. Martinho, A. Santos, A. Fedorov, R. Baptista, M. Taipa, J. Cabral, Fluorescence of the single tryptophan of cutinase: temperature and pH effect on protein conformation and dynamics, Photochem. Photobiol. 78 (2003) 15–22.
[40] D.W. Marquardt, An algorithm for least squares estimation of nonlinear parameters, J. Soc. Ind. Appl. Math. 11 (1963) 431–441.
[41] T. Förster, Zwischenmolekulare energiewanderung und fluoreszenz, Ann. Physik 437 (1948) 55–75.
[42] M.L. Johnson, CFS_LS, Non-Linear Least-Squares Fitting Program, Center for Fluorescence Spectroscopy, Baltimore, MD, 2000.
[43] T.Q. Faria, J.C. Lima, M. Bastos, A.L. Maçanita, H. Santos, Protein stabilization by osmolytes from hyperthermophiles, J. Biol. Chem. 279 (2004) 48680–48691.
[44] A.G. Szabo, D.M. Rayner, Fluorescence decay of tryptophan conformers in aqueous solution, J. Am. Chem. Soc. 102 (1980) 554–563.
[45] Y. Chen, M.D. Barkley, Toward understanding tryptophan fluorescence in proteins, Biochemistry 37 (1998) 9976–9982.
[46] C. Magg, F.X. Schmid, Rapid collapse precedes the fast two-state folding of the cold shock protein, J. Mol. Biol. 335 (2004) 1309–1323.
[47] E. James, P.G. Wu, W. Stites, L. Brand, Compact denatured state of a staphylococcal nuclease mutant by guanidinium as determined by resonance energy transfer, Biochemistry 31 (1992) 10217–10225.